

Measurement of the spin-dependent parameters D , R , A , and P for small-angle p - p elastic scattering between 300 and 600 MeV

D. Besset,* Q. H. Do, B. Favier, L. G. Greeniaus,[†] R. Hess, C. Lechanoine, D. Rapin, and D. W. Werren[‡]

Département de Physique Nucléaire et Corpusculaire, University of Geneva, Geneva, Switzerland

Ch. Weddigen

Institut für Kernphysik, Kernforschungszentrum und Universität Karlsruhe, Karlsruhe, Federal Republic of Germany

(Received 23 July 1979; revised manuscript received 22 January 1980)

The Wolfenstein parameters D , R , and A and the polarization parameter P have been measured for p - p elastic scattering at 312, 392, 493, and 575 MeV kinetic energy. The center-of-mass angular range observed was from 3° to 33° . The experiment was performed at SIN, using a polarized proton beam. These data significantly improve the determination of $I = 1$ phase shifts.

I. INTRODUCTION

For nucleon-nucleon scattering, the intermediate energy region above 300 MeV is particularly interesting. The spin-averaged total cross section rises strongly with energy, the π -production threshold opens at 290 MeV, and spin-dependent effects vary rapidly with scattering angle and energy. Also, recent measurements of the p - p total-cross-section difference with longitudinally polarized beam and target¹⁻³ suggest the existence of two nucleon resonances.

To date, no satisfactory theoretical description of the N - N interaction exists above 330 MeV. At lower energies, progress in the construction of a realistic semiphenomenological nucleon-nucleon interaction by the Paris NN group⁴ has been made, while at higher energies, quark and parton models have had a good deal of success. In the intermediate energy region, some results have been obtained recently from the MIT bag model,⁵ but a quantitative description of the dynamics of quarks has yet to be achieved. In the absence of a working theory, it has been common practice to use phenomenological phase-shift analyses to fit the experimental data. The reliability of this method depends both on the inherent assumptions involved and upon the quality and the amount of experimental data. Data for rarely measured complex polarization parameters are important as they provide information about the relative magnitudes and phases of individual amplitudes. Also important are measurements at small scattering angles ($\theta_{c.m.} \approx 5^\circ$). These provide information concerning Coulomb-nuclear interference effects. For example, differential-cross-section measurements in this region measure the ratio of the real and imaginary parts of the non-spin-flip nuclear forward amplitude.⁶ Polarization measurements here may be used to obtain infor-

mation on some of the nuclear amplitudes.⁷ This angular region is also sensitive to high angular momentum values and to the pion-exchange contributions to the N - N interaction.

Apart from $d\sigma/d\Omega$, there are 24 other linearly independent observables involving polarization parameters. Only nine of these have been measured⁸ up to now; almost none of these measurements were done in the Coulomb-nuclear interference region.

One set of parameters $D(D_{n_0n_0})$, $R(D_{s'_0s_0})$, $R'(D_{k'_0s_0})$, $A(D_{s'_0k_0})$, $A'(D_{k'_0k_0})$, and $P(A_{00n_0}$ and $P_{n_000})$ describe how the proton polarization is affected by a scattering on an unpolarized proton target. (The four-subscript notation used to denote general experimental quantities has been developed and studied in great detail by Bystricky *et al.*⁹ For ease of presentation we use the conventional notation of Wolfenstein in this article, except when we wish to distinguish the analyzing power A_{00n_0} and polarization P_{n_000} parameters.) In this experiment we limit ourselves to measurements of D , R , A , and P , the parameters which concern the transverse component of polarization of scattered protons. Results are presented here for the angular range including the Coulomb-nuclear interference region $3^\circ \leq \theta_{c.m.} \leq 33^\circ$ at 312, 392, 493, and 575 MeV (kinetic energy at the center of the hydrogen target). The good angular resolution achieved permitted observation of strongly varying angular dependence of the observables. Statistical errors, typically $\approx \pm 0.08$ on D , R , and A and $\leq \pm 0.02$ on P in 2° c.m. bins, have been obtained. Systematic errors are small.

II. PRINCIPLE OF THE MEASUREMENT

A. Principle of data taking

We performed a conventional double-scattering experiment using an incident proton beam with a

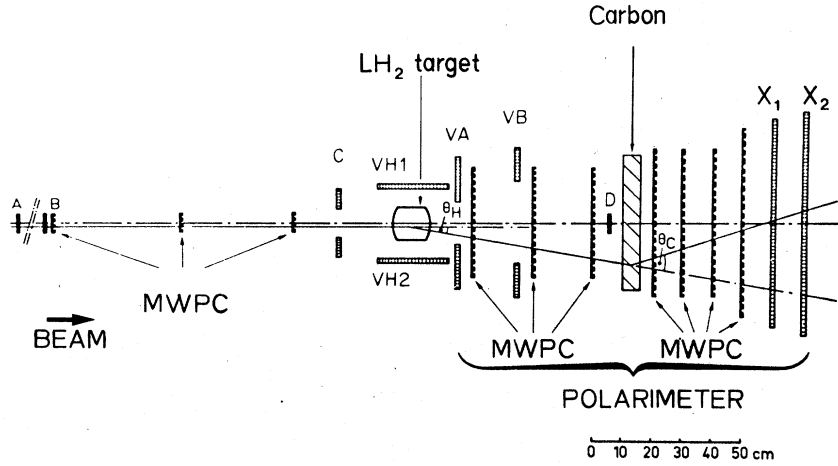


FIG. 1. Scale drawing of the apparatus. MWPC's are multiwire proportional chambers, and A, B, C, D, X₁, X₂, VH1, VH2, VA, and VB are scintillation counters.

transverse or longitudinal polarization. The experimental setup is shown in Fig. 1. After a first scattering from a liquid-hydrogen (LH₂) target, the full azimuthal distribution of the forward scattered proton was observed. The associated recoil proton usually had too low an energy to get out of the target. The transverse polarization of the elastically scattered protons was then measured by observing the azimuthal distribution after a second scattering from a carbon analyzer (C). Again here the full azimuthal distribution is observed.

The two scattering targets (LH₂ and C) were sandwiched between multiwire-proportional-chamber (MWPC) telescopes placed directly into the beam. This configuration restricted the permissible beam intensity to $\approx 2 \times 10^5$ p/s, thus limiting the data-acquisition rate. A fast electronic system¹⁰ selected the rare double-scattered events. The probability of having both scatterings in the interesting angular region was $\approx 10^{-4}$. Inelastically scattered events from the LH₂ target were rejected by time-of-flight (TOF) and dE/dx measurements as well as by veto counters placed around the target. It should be noted that this experimental setup also allows a measurement of single scattering on carbon. A detailed description of the apparatus is given in Sec. III.

B. Principle of data analysis

1. General formalism

Let us consider an incident proton beam moving along the \hat{Z} direction with a polarization

$$\vec{P}_b = P_x \hat{X} + P_y \hat{Y} + P_z \hat{Z}. \quad (1)$$

Scattering from an unpolarized hydrogen target

(subscript H) produces an azimuthal distribution proportional to

$$\begin{aligned} I_H(\theta_H, \phi_H) &= I_{0H}(\theta_H) [1 + A_{00n0}(\theta_H) \vec{P}_b \cdot \hat{n}_H] \\ &= I_{0H}(\theta_H) [1 + \epsilon_{1n}(\theta_H) \cos \phi_H \\ &\quad + \epsilon_{1s}(\theta_H) \sin \phi_H], \end{aligned} \quad (2)$$

where I_{0H} is the distribution observed with an unpolarized beam. The definitions of the coordinate axis and angles for the first scattering are shown in Fig. 2. Notice that the reference axes \hat{n} , \hat{s}' , \hat{k}' defined by the first scattering are changing for each θ_H, ϕ_H value.

The outgoing polarization of the scattered proton $\langle \vec{\sigma} \rangle$ can be expressed as a function of the Wolfenstein parameters:

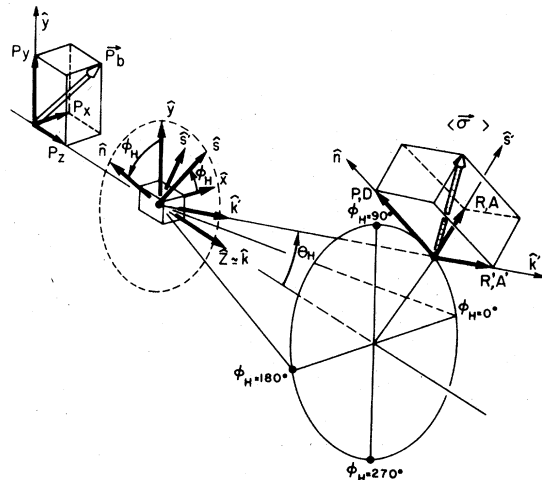


FIG. 2. Definition of reference axes used for the first scattering on hydrogen.

$$\langle \vec{\sigma} \rangle = \frac{1}{1 + \vec{P}_b \cdot \hat{n} A_{00n0}(\theta_H)} \{ [P_{n000}(\theta_H) + D_{n0n0}(\theta_H) \vec{P}_b \cdot \hat{n}] \hat{n} + [D_{s'0k0}(\theta_H) \vec{P}_b \cdot \hat{k} + D_{s'0s0}(\theta_H) \vec{P}_b \cdot \hat{s}] \hat{s}' + [D_{k'0k0}(\theta_H) \vec{P}_b \cdot \hat{k} + D_{k'0s0}(\theta_H) \vec{P}_b \cdot \hat{s}] \hat{k}' \}. \quad (3)$$

Parity and time-reversal conservation imply that the polarization and analyzing power are equal. They are denoted by P :

$$P_{n000} \equiv A_{00n0} \equiv P. \quad (4)$$

Figure 3 illustrates at 392 and 575 MeV how the transverse polarization of a 100% vertically polarized proton beam is affected in a scattering on an unpolarized proton target as a function of the scattering angles $\theta_{c,m}$ and ϕ . The direction and magnitude of the arrows illustrate the combined effect of P , D , and R . This also shows that spin-dependent effects vary rapidly with scattering angle and energy.

The transverse-polarization components along the \hat{n} and \hat{s}' axes of the scattered proton can be measured by a second scattering on carbon. A formula analogous to Eq. (2) describes the distribution after the second scattering on carbon (subscript C):

$$I_C(\theta_H, \phi_H, \theta_C, \phi_C) = I_H(\theta_H, \phi_H) I_{0C}(\theta_C) [1 + P_C(\theta_C) \langle \vec{\sigma} \rangle \cdot \hat{n}_C], \quad (5)$$

where $P_C(\theta_C)$ is the carbon analyzing power, and I_{0C} the distribution for scattering of unpolarized particles on carbon.

If \hat{k}'' is the direction of the outgoing particle after scattering on carbon, the reference axes can be defined by

$$\hat{n}_C = \frac{\hat{k}' \times \hat{k}''}{|\hat{k}' \times \hat{k}''|}, \quad \cos \phi_C = \hat{n}_C \cdot \hat{n}, \quad \sin \phi_C = -\hat{n}_C \cdot \hat{s}'. \quad (6)$$

The azimuthal distribution after the second scattering for a given θ_H becomes

$$I_C(\theta_H, \phi_H, \theta_C, \phi_C) = I_H(\theta_H, \phi_H) I_{0C}(\theta_C) [1 + \langle \sigma(\theta_H, \phi_H) \rangle_n P_C(\theta_C) \cos \phi_C - \langle \sigma(\theta_H, \phi_H) \rangle_s P_C(\theta_C) \sin \phi_C] \\ = I_H(\theta_H, \phi_H) I_{0C}(\theta_C) [1 + \epsilon_{2n}(\theta_H, \phi_H, \theta_C) \cos \phi_C + \epsilon_{2s}(\theta_H, \phi_H, \theta_C) \sin \phi_C], \quad (7)$$

where $\langle \sigma \rangle_n$ and $\langle \sigma \rangle_s$ are given by

$$\langle \sigma \rangle_n = \frac{P(\theta_H) + D(\theta_H)(P_Y \cos \phi_H - P_X \sin \phi_H)}{1 + P(\theta_H)(P_Y \cos \phi_H - P_X \sin \phi_H)}, \quad (8) \\ \langle \sigma \rangle_s = + \frac{P_Z A(\theta_H) + R(\theta_H)(P_Y \sin \phi_H + P_X \cos \phi_H)}{1 + P(\theta_H)(P_Y \cos \phi_H - P_X \sin \phi_H)}.$$

The $A'(D_{k'0k0})$ and $R'(D_{k'0s0})$ parameters disappear in the scalar product $\langle \vec{\sigma} \rangle \cdot \hat{n}_C$.

2. General analysis

In the first scattering, defined by Eq. (2), the asymmetries $\underline{\epsilon}_1$ are given by the products

$$\underline{\epsilon}_1 = \begin{bmatrix} P_Y P(\theta_H) \\ -P_X P(\theta_H) \end{bmatrix} = P_b P(\theta_H) \begin{bmatrix} P_Y/P_b \\ -P_X/P_b \end{bmatrix}. \quad (9)$$

As the ratios P_Y/P_b and P_X/P_b are constants which depend only on the orientation of the beam polarization, these asymmetries measure the product

$$\alpha = P_b P(\theta_H). \quad (10)$$

For the second scattering, at a fixed θ_H , the

asymmetries given in Eqs. (7) and (8) can be rewritten in a way similar to Eq. (9), putting into evidence the beam polarization P_b :

$$\langle \sigma \rangle_n P_C(\theta_C) = \epsilon_{2n}(\theta_C) = C(\phi_H) P_b P_C(\theta_C), \quad (11)$$

$$-\langle \sigma \rangle_s P_C(\theta_C) = \epsilon_{2s}(\theta_C) = S(\phi_H) P_b P_C(\theta_C), \quad (12)$$

with

$$C(\phi_H) = \frac{P/P_b + D(\cos \phi_H P_Y/P_b - \sin \phi_H P_X/P_b)}{1 + P P_b (\cos \phi_H P_Y/P_b - \sin \phi_H P_X/P_b)}, \quad (13)$$

and

$$S(\phi_H) = \frac{-AP_Z/P_b - R(P_Y/P_b \sin \phi_H + P_X/P_b \cos \phi_H)}{1 + P P_b (\cos \phi_H P_Y/P_b - \sin \phi_H P_X/P_b)}. \quad (14)$$

For calibration purposes, when only single scattering from carbon is studied, the observed azimuthal distribution is similar to Eq. (2):

$$I_C(\theta_C, \phi_C) = I_{0C}(\theta_C) \left[1 + \frac{P_Y}{P_b} P_b P_C(\theta_C) \cos \phi_C - \frac{P_X}{P_b} P_b P_C(\theta_C) \sin \phi_C \right]. \quad (15)$$

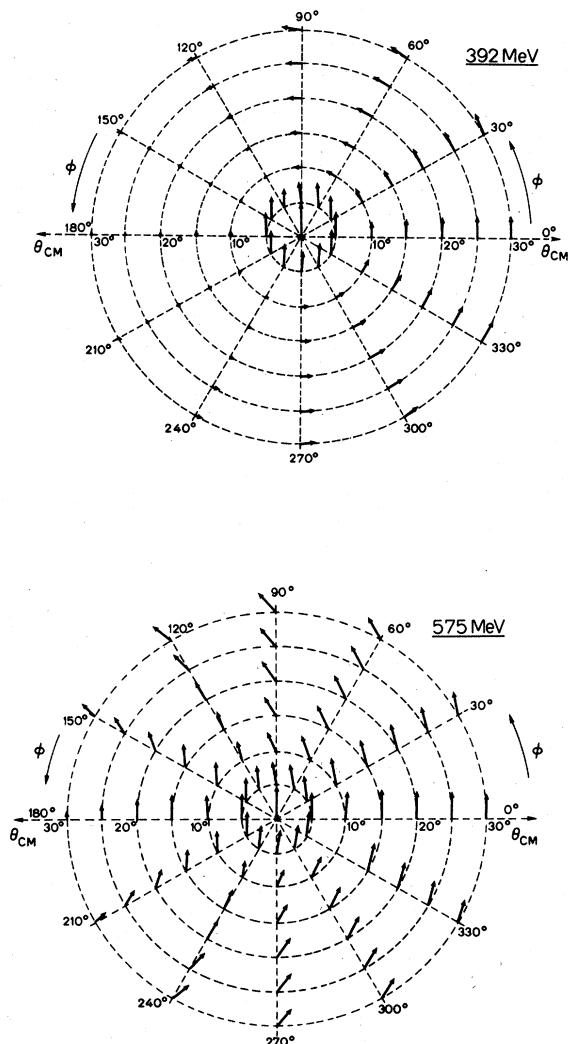


FIG. 3. A representation of the transverse polarization of a 100% vertically polarized proton beam scattered from an unpolarized target at 392 and 575 MeV as a function of the scattering angles ($\theta_{\text{c.m.}}, \phi$). The direction and magnitude of the arrows illustrate the combined effect of P , D , and R .

This allows measurement of the quantity

$$P_a(\theta_C) = P_b P_C(\theta_C) \quad (16)$$

in the same experimental conditions as for the polarization analysis of the protons scattered from the LH_2 target. Defining the quantity

$$\beta = P(\theta_H) / P_b, \quad (17)$$

a statistical analysis of the ϕ_H dependence of the second scattering asymmetries ϵ_2 [see Eqs. (11–14)], using the values of α and $P_a(\theta_C)$, allows β , $D(\theta_H)$, $R(\theta_H)$, and $A(\theta_H)$ to be determined. The beam polarization P_b can then be deduced from the

quantities α and β .

The experiment was completely self-consistent. It measured all parameters including the carbon analyzing power, and the beam polarization. It was not necessary to introduce results from any other experiments. The complete analysis procedure will be discussed in detail in Sec. IV B.

III. EXPERIMENTAL METHOD

A complete description of the beam and experimental apparatus can be found in Refs. 11–13.

A. Beam transport

The polarized beam at SIN (PM1 channel) has two modes of operation. In its parasitic mode, the main unpolarized beam (590-MeV proton) is scattered at 8° off a thin beryllium target. It is then deflected and analyzed by two magnets and directed to the experimental area. In single user mode, protons originating from the SIN polarized source are accelerated to 590 MeV and deflected magnetically into the PM1 channel.

A variable-thickness copper degrader located in between the two magnets is used to lower the beam energy. Theoretical calculations predict that the beam degrader and transport system should have negligible depolarization effects. This was confirmed experimentally as discussed in Sec. V B.

The beam energies have been determined by using the kinematic relation between the π and the d tracks for $pp \rightarrow \pi^+ d$ events¹⁴ which were recorded separately for this purpose. Typical statistical errors in determining the mean energy at the target center were ± 2 MeV.

A combination of a magnet and solenoid allowed either a longitudinally or transversally polarized beam, depending on their relative positions. In the early stages of the experiment the large superconducting solenoid, capable of rotating the polarization vector of a 590-MeV proton beam by 180° , was not operational. A smaller superconducting solenoid plus a conventional solenoid were used instead. This combination was capable of rotating the polarization vector by any angle ϕ_0 up to a maximum of 54° to 78° , depending on the beam energy (see Table I). Thus there was always a small transverse polarization component with the longitudinally polarized beam. One drawback of the temporary two-solenoid arrangement was that it was not possible to completely reverse the spin unless the accelerated polarized beam was used. As this mode of operation is rarely available at SIN (one week a year), only the 575-MeV data were accumulated using this beam. A summary of the beam polarization orientations is given in Table I.

TABLE I. Summary of the beam polarization components along the X , Y , and Z axes, as well as the rotation angle φ_0 in the solenoids in (a) for data taken with the scattered beam at 312, 493, and 575 MeV, in (b) for data taken with the scattered beam at 392 MeV, and in (c) for data taken with the accelerated polarized beam at 575 MeV.

	(a) Scattered beam								
	312 MeV			493 MeV			575 MeV		
	P_X/P_b	P_Y/P_b	P_Z/P_b	P_X/P_b	P_Y/P_b	P_Z/P_b	P_X/P_b	P_Y/P_b	P_Z/P_b
Transversal beam	± 0.977	$+0.212$	0	± 0.865	0.502	0	no data		
Longitudinal beam	0	$+0.218$	± 0.976	0	0.504	± 0.863	0	0.581	± 0.813
φ_0 (degrees) solenoid rotation angle	± 77.75			± 59.85			± 54.66		
	(b) Scattered beam 392 MeV			(c) Accelerated beam 575 MeV					
	P_X/P_b	P_Y/P_b	P_Z/P_b	P_X/P_b	P_Y/P_b	P_Z/P_b	P_X/P_b	P_Y/P_b	P_Z/P_b
Transversal beam	0	1	0	Transversal beam	-0.816	-0.578	-0.816	$+0.578$	0
	0	0.788	± 0.615		$+0.816$	$+0.578$	$+0.816$	-0.578	
Longitudinal beam	0	0.375	± 0.927		0	$+1$	0	$+1$	
	0	0	± 1		0	-1			
φ_0 (degrees)	0, ± 38 , ± 68 , ± 90			φ_0 (degrees)	± 54.66				

B. Detection apparatus

The apparatus consisted of three MWPC telescopes which observed individual particle trajectories on both sides of the 12-cm-long liquid-hydrogen target and the 5-cm-thick carbon target (see Fig. 1). At 312 MeV, only 4 cm of carbon were used. A total of 10 MWPC's providing horizontal (X) and vertical (Y) coordinates were used. The chamber farthest downstream was rotated by 11° about the beam axis to resolve ambiguities due to multiple tracks in the backward telescope. Scintillation counters A , B , \bar{C} , \bar{D} , X_1 , and X_2 were used to trigger the readout chamber system. Times of flight (TOF's between B and $X_1 X_2$ and the dE/dx in X_1 and X_2 were measured. The counters $VH1$, $VH2$, VA , and VB were used to reject inelastic events such as $pp \rightarrow \pi^+ d$, $pp \rightarrow np\pi^+$, and $pp \rightarrow pp\pi^0$ in the off-line analysis.

C. Data acquisition

An event selection was necessary, as the probability of a double scattering in the interesting angular region is $\approx 10^{-4}$. A special electronics system^{10,13} connected to the coding system of the MWPC's was built for this purpose. The selection was done on the basis of the values of the projected scattering angles and on the number of

coded wire clusters per plane. The upper limits for rejectable scattering angles were 2° and 5° in the laboratory for the hydrogen and carbon scattering, respectively. Events for which no decision could be made due to too many coordinates were accepted by default and also transferred to a PDP 11/20 as the accepted ones.

Each event had to satisfy other on-line conditions however, before it could be recorded on magnetic tape. These tests were the following:

(i) Since the intermediate telescope took part in the decision logic for the two scatterings, particular attention was paid to eliminate any ill behavior in any of its three MWPC's since such poor operating conditions could result in simulated double scatterings. For each X and Y projection in the three telescopes, a straight line was calculated using the information from two of the planes having a single coordinate. The equal spacing of chambers greatly simplified these calculations. The distance between the calculated straight-line projections and the coordinates in the third, unused, plane had to be within 4 mm. This test rejected 55% of the events in the front and middle telescopes. These bad events were due primarily to the simultaneous occurrence of an inefficiency and a parasitic spark in a chamber. Both probabilities were $\approx 10^{-2}$. In the rear telescope, if no

alignment was possible, the event was written on magnetic tape for off-line analysis.

(ii) Events with a laboratory scattering angle from the hydrogen greater than 15° or smaller than 1° were rejected.

(iii) The distance of closest approach between the incident and outgoing tracks on the LH_2 target was limited to < 6 mm. The reconstructed event origin also had to lie in or close to the LH_2 target.

These three cuts eliminated $\approx 80\%$ of the events. After the overall selection including hardware and software requirements, events written on magnetic tape were 3×10^{-4} of the gated ABC triggers. About 600 magnetic tapes, each with $\sim 130\,000$ events, were recorded. Three different types of data were considered for each energy, as reported in Table II. For the carbon and double-scattering data, approximately equal numbers of events were acquired for each direction of beam polarization. (These various beam conditions are summarized in Table I.)

At 575 MeV, which was taken with the beam originating from the polarized ion source, data acquisition was different. As it was necessary to monitor the beam polarization continuously to observe its short-term fluctuations, we swapped between p - p double-scattering and p -C single-scattering conditions every minute or so by changing programmable parameters in CAMAC modules.¹³

IV. DATA ANALYSIS

A. Off-line reconstruction

(i) In the off-line analysis the recorded events were required to meet six supplementary conditions before being used to determine P , D , R , and A . Altogether these six conditions reduced the number of events by an additional factor of 3.

As false asymmetries in the experiment are very sensitive to errors in specification of the MWPC's location, these positions were determined

with great care. Special calibration data, with no scattering on carbon, were recorded for that purpose as indicated in Table II. For each of the 20 planes, five misalignment parameters were considered: one transverse displacement (Δx or Δy), one longitudinal displacement (Δz), and three angle rotations ($\Delta\phi_x, \Delta\phi_y, \Delta\phi_z$) corresponding to the five possible degrees of freedom. Two chambers (two x planes, two y planes) were taken as a reference and a least-squares procedure was used to determine the parameters for the other planes. The equations to be solved are linear for small displacements.

The raw coordinates were first corrected for the relative geometrical displacements of the MWPC's from their nominal positions. The trajectories in all three telescopes were then recalculated. For the rear telescope a χ^2 figure of merit defined by

$$\chi^2 = \frac{1}{n-4} \sum_{i=1}^n (f_m^i - f^i)^2 < 4 \text{ mm}^2 \quad (18)$$

was also calculated. The f 's are the measured or calculated coordinates defined as the intersection of the computed trajectory with the i th plane, and n is the number of planes used in the reconstruction. Events without a trajectory or with more than one trajectory reconstructed were rejected ($\approx 4\%$).

(ii) The beam size at the middle of the LH_2 target was limited to a circle of 30 mm radius and a beam divergence ≤ 20 mrad was required in order to facilitate acceptance considerations.

(iii) The determination of the interaction point along the beam axis, defined by the incident and scattered tracks, has an experimental uncertainty which depends on the scattering angle. For the hydrogen vertex, we applied an angle-dependent cut in order to optimize the elimination of events scattered on the Mylar windows. However, the number of events scattered from the upstream

TABLE II. Summary of the different types of data registered at each energy.

Type of data	Experimental conditions	Aim
Calibration	Straight tracks Single scattering on an aluminum plate behind empty LH_2 target	To align the MWPC (see Sec. IV A) and map correction for TOF and dE/dX in X_1 and X_2 counters (see Ref. 13)
Carbon	Single scattering on carbon	To measure $P_b P_c$
Hydrogen	Double scattering: first on hydrogen, then on carbon	To measure P , D , R , A , and P_b

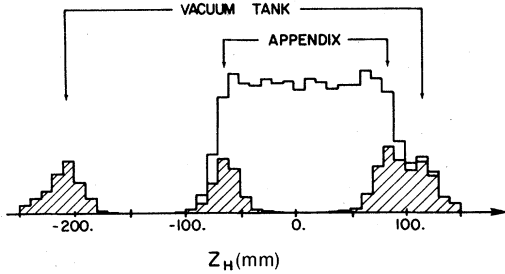


FIG. 4. Distribution of the interaction vertex in the LH_2 target (Z_H) along the beam axis at 312 MeV for $6^\circ < \theta_{\text{lab}} < 9^\circ$. The shaded area corresponds to empty target data normalized to the same number of incident particles as for the LH_2 data.

window was counted separately and used to normalize the target-full to target-empty data. A typical vertex distribution is shown in Fig. 4. For the carbon vertex, a constant cut could be applied since even at the smallest scattering angle considered, the vertex resolution was good.

(iv) The minimum squared distance between the incoming and the outgoing tracks had to be $< 15 \text{ mm}^2$ for the hydrogen vertex and $< 20 \text{ mm}^2$ for the carbon scattering.

(v) Measurements of time of flight and energy loss in the X counters were used to eliminate events due to inelastic reactions. The measured values of TOF and dE/dx were corrected for time drifts, time slewing, and spatial dependence on the impact point in the counters. After these corrections (explained in detail in Refs. 11 and 13), the TOF and dE/dx for elastically scattered events were independent of both the impact point in the X counters and the scattering angle. A TOF resolution of 320 psec full width at half maximum (FWHM) was achieved. For the dE/dx , the resolution was 20% FWHM. An excellent rejection of the two-body inelastic events $pp \rightarrow \pi^+ d$ was achieved.

Another source of contamination was due to three-body inelastic reactions which produce particles having a continuous velocity spectrum extending into the region of the elastically scattered protons. These were almost completely eliminated by using the additional information from the veto counters $VH1$, $VH2$, VA , and VB . Figure 5 shows a typical corrected TOF- dE/dx plot. The data were cut as shown by the shaded areas in order to reject inelastic events.

For laboratory scattering angles $\theta_H < 11^\circ$, events which triggered any of the veto counters were rejected. For $\theta_H > 11^\circ$, only information from VA and VB was used as the cylindrical counters $VH1$, $VH2$ placed around the target often detected the

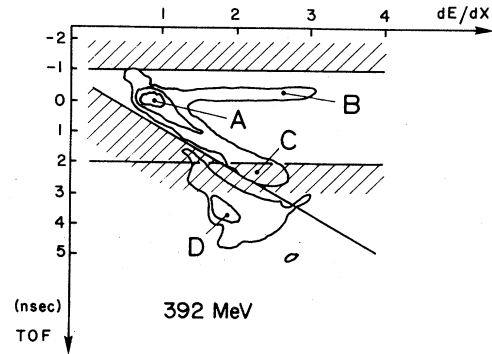


FIG. 5. TOF vs dE/dX at 392 MeV for events not hitting the veto counters. The contours represent increments of counts of a factor 10. The letters A, B, C, D stand for pp elastic, interaction in the X counters, p -C inelastic scattering, and $pp \rightarrow \pi d$ events. The scale for TOF is calculated as the difference between the TOF of an event and the one for elastically scattered protons. The scale for dE/dX is the ratio between the dE/dX and the one for elastic protons. Details can be found in Ref. 12.

recoil proton in the elastic scattering. For smaller angles, the recoil particle did not have sufficient energy to escape from the target. A detailed study of veto counters can be found in Ref. 12.

B. Parameter evaluation

This section is a detailed treatment of the ideas expressed in Sec. II B 2. Since the analysis is made at a fixed hydrogen scattering angle θ_H , this variable will be left out of the equations for simplicity. For these calculations, the system acceptance function $A(\phi_H, \theta_C, \phi_C)$ was taken into account as a multiplicative factor on the right-hand side of Eq. (5). Our analysis is based on the known symmetry properties of this acceptance function. Different types of acceptance, corresponding to different symmetry properties, were defined for the study of both the first scattering on hydrogen and the second scattering on carbon. The acceptance used to evaluate the data presented in Ref. 15 will not be discussed here, as it is valid for a very restrictive angular domain ($\theta_{\text{H.c.m.}} < 15^\circ$).

1. Asymmetries from the hydrogen scattering

Events used to determine the hydrogen-scattering asymmetry must be detected independently of ϕ_C . That is, the acceptance must have the form

$$A(\phi_H, \theta_C) = A(\phi_H + \pi, \theta_C) \quad (19)$$

for $0 \leq \phi_C < 2\pi$. In Ref. 16 we discuss how to find efficient estimators of measured asymmetries or

polarization components with acceptance functions that are the same for ϕ and $\phi + \pi$. These are very convenient to use in the case of an experimental setup having a π -symmetric acceptance function in ϕ . To apply these estimators, the basic condition is that the event and its "anti-event" characterized by $(\phi_H + \pi, \theta_C)$ must be detectable in the rear telescope for all $0 \leq \Phi_C < 2\pi$ [see Fig. 6(a)]. Figure 6(c) shows the number of detected events as a function of θ_H for this so-called "restricted" acceptance condition as well as for all the reconstructed events (see Sec. IV A).

Under these conditions, the asymmetries ϵ_{1n} , ϵ_{1s} after the first scattering [see Eqs. (2) and (8)] can be calculated with the estimators¹⁶

$$\begin{pmatrix} \hat{\epsilon}_{1n} \\ \hat{\epsilon}_{1s} \end{pmatrix} = \begin{pmatrix} \sum_{\sigma\nu} \cos^2 \phi_H & \sum_{\sigma\nu} \sin \phi_H \cos \phi_H \\ \sum_{\sigma\nu} \sin \phi_H \cos \phi_H & \sum_{\sigma\nu} \sin^2 \phi_H \end{pmatrix}^{-1} \times \begin{pmatrix} \sum_{\sigma\nu} \cos \phi_H \\ \sum_{\sigma\nu} \sin \phi_H \end{pmatrix} \quad (20)$$

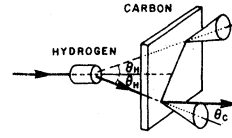
or in matrix form $\hat{\xi}_1 = \underline{F}^{-1} \underline{B}$. The sums are made over all events inside same θ_H bins (all θ_C , all ϕ_C , all ϕ_H). The associated covariance matrix is

$$\underline{V}(\hat{\xi}_1) = \underline{F}^{-1}. \quad (21)$$

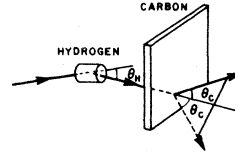
2. Asymmetries for the second scattering on carbon

The polarization components of the particles scattered from the hydrogen target are estimated by this scattering. Two different types of acceptance functions can be considered, leading to completely different methods of computation. Consistency of results obtained with these two different acceptances is a good self-consistent check.

(i) "Restricted" acceptance [as defined in Eq. (19)]. For the second scattering, the symmetry



a) Restricted acceptance



b) Large acceptance

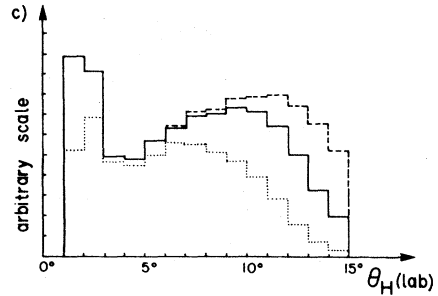


FIG. 6. Conditions for the two different types of acceptance considered. (a) and (b) show a typical event (in full lines) and the symmetry requirement imposed (dotted lines). (c) shows the number of accepted events as a function of the laboratory scattering angle θ_H for the overall reconstructed events (dashed line), events satisfying to the "large" acceptance conditions (full line) and the events satisfying the "restricted" acceptance (dotted line).

property of the acceptance given in Eq. (19) allows simplified calculations since

$$\int_0^{2\pi} A(\phi_H, \theta_C) \sin^m \phi_H \cos^n \phi_H d\phi_H = 0 \quad (22)$$

if $n+m$ is odd. Then the estimation of integrals by calculating sums over a sample of N events such as

$$\int d\theta_C \int_0^{2\pi} d\phi_H \int_0^{2\pi} I_C(\phi_H, \theta_C, \phi_C) A(\phi_H, \theta_C) P_a(\theta_C) \cos \phi_H \cos \phi_C d\phi_C = \sum_{\sigma\nu} P_a(\theta_C) \cos \phi_H \cos \phi_C \quad (23)$$

allows a direct determination of the Wolfenstein parameters if $P_a(\theta_C) = P_b P_C(\theta_C)$ is known.¹² The sum is done over all events inside same θ_H bins (all θ_C , all ϕ_C , all ϕ_H). One gets in a matrix

form, for the D and R parameters,

$$\underline{B}_D = \underline{F} \underline{\epsilon}_D, \quad \underline{B}_R = \underline{F} \underline{\epsilon}_R \quad (24)$$

with

$$\underline{B}_D = \begin{pmatrix} \sum_{\epsilon\nu} P_a(\theta_C) \cos\phi_H \cos\phi_C \\ \sum_{\epsilon\nu} P_a(\theta_C) \sin\phi_H \cos\phi_C \end{pmatrix}, \quad \underline{\epsilon}_D = \begin{pmatrix} DP_Y/P_b \\ -DP_X/P_b \end{pmatrix}, \quad \underline{B}_R = \begin{pmatrix} \sum_{\epsilon\nu} P_a(\theta_C) \cos\phi_H \sin\phi_C \\ \sum_{\epsilon\nu} P_a(\theta_C) \sin\phi_H \sin\phi_C \end{pmatrix}, \quad \underline{\epsilon}_R = - \begin{pmatrix} RP_X/P_b \\ RP_Y/P_b \end{pmatrix}, \quad (25)$$

$$\underline{F} = \begin{pmatrix} \frac{1}{2} \sum_{\epsilon\nu} P_a(\theta_C)^2 \cos^2\phi_H & \frac{1}{2} \sum_{\epsilon\nu} P_a(\theta_C)^2 \sin\phi_H \cos\phi_H \\ \frac{1}{2} \sum_{\epsilon\nu} P_a(\theta_C)^2 \sin\phi_H \cos\phi_H & \frac{1}{2} \sum_{\epsilon\nu} P_a(\theta_C)^2 \sin^2\phi_H \end{pmatrix}. \quad (27)$$

The covariance matrix in both cases is given by a formula of the form

$$\underline{V}(\underline{\epsilon}) = \underline{F}^{-1} \underline{V}(\underline{B}) \underline{F}^{-1} \quad (28)$$

with

$$\underline{V}(\underline{B}) = \underline{F}. \quad (29)$$

The P/P_b and A parameters are estimated by the following equations:

$$\begin{aligned} 2 \sum_{\epsilon\nu} P_a(\theta_C) \cos\phi_C &= P/P_b \sum_{\epsilon\nu} P_a(\theta_C)^2, \\ 2 \sum_{\epsilon\nu} P_a(\theta_C) \sin\phi_C &= -AP_z/P_b \sum_{\epsilon\nu} P_a(\theta_C)^2. \end{aligned} \quad (30)$$

TABLE III. Summary of the sums necessary to estimate the asymmetries in the first scattering on hydrogen (subscript H), and in the second scattering on carbon (subscript C) for the two acceptance functions discussed in Sec. IV B. P_a is the product of the beam polarization P_b times the carbon analyzing power P_C .

	"Restricted" acceptance	"Large" acceptance
First scattering	$\sum \cos^2\phi_H$	
	$\sum \sin^2\phi_H$	
	$\sum \sin\phi_H \cos\phi_H$	
	$\sum \cos\phi_H$	
	$\sum \sin\phi_H$	
Second scattering	$\sum P_a(\theta_C)^2 \cos^2\phi_H$	$\sum P_a(\theta_C) \sin\phi_C$
	$\sum P_a(\theta_C)^2 \sin^2\phi_H$	$\sum P_a(\theta_C) \cos\phi_C$
	$\sum P_a(\theta_C)^2 \sin\phi_H \cos\phi_H$	$\sum P_a(\theta_C)^2 \cos^2\phi_C$
	$\sum P_a(\theta_C) \cos\phi_C$	$\sum P_a(\theta_C)^2 \sin^2\phi_C$
	$\sum P_a(\theta_C) \sin\phi_C$	$\sum P_a(\theta_C)^2 \sin\phi_C \cos\phi_C$
	$\sum P_a(\theta_C) \cos\phi_C \sin\phi_H$	$\sum P_a(\theta_C)^2 \cos^2\phi_C (\phi_H - \phi_0)$
	$\sum P_a(\theta_C) \cos\phi_C \cos\phi_H$	$\sum P_a(\theta_C)^2 \sin^2\phi_C (\phi_H - \phi_0)$
	$\sum P_a(\theta_C) \sin\phi_C \sin\phi_H$	$\sum P_a(\theta_C)^2 \sin\phi_C \cos\phi_C (\phi_H - \phi_0)$
	$\sum P_a(\theta_C) \sin\phi_C \cos\phi_H$	$\sum P_a(\theta_C)^2 \cos^2\phi_C (\phi_H - \phi_0)^2$
		$\sum P_a(\theta_C)^2 \sin^2\phi_C (\phi_H - \phi_0)^2$
		$\sum P_a(\theta_C)^2 \sin\phi_C \cos\phi_C (\phi_H - \phi_0)^2$
		$\sum P_a(\theta_C) \sigma'_C / \sigma_C \cos^2\phi_C$
		$\sum P_a(\theta_C) \sin\phi_C \cos\phi_C \sigma'_C / \sigma_C$
	$\sum P_a(\theta_C) \sin^2\phi_C \sigma'_C / \sigma_C$	

Table III summarizes the necessary sums to be calculated in order to estimate the Wolfenstein parameters for the first and the second scattering if this so called restricted acceptance is used.

(ii) "Large" acceptance. Equation (19) is in fact too restrictive, as the second scattering asymmetries can be studied without making any requirement on the first scattering acceptance if one chooses an acceptance function such that

$$A(\phi_H, \theta_C, \phi_C) = A(\phi_H, \theta_C, \phi_C + \pi) \quad (31)$$

$$\begin{bmatrix} \hat{C}(\phi_H) \\ \hat{S}(\phi_H) \end{bmatrix} = \begin{bmatrix} \sum_{\text{ev}} P_a(\theta_C)^2 \cos^2 \phi_C & \sum_{\text{ev}} P_a(\theta_C)^2 \sin \phi_C \cos \phi_C \\ \sum_{\text{ev}} P_a(\theta_C)^2 \sin \phi_C \cos \phi_C & \sum_{\text{ev}} P_a(\theta_C)^2 \sin^2 \phi_C \end{bmatrix}^{-1} \begin{bmatrix} \sum_{\text{ev}} P_a(\theta_C) \cos \phi_C \\ \sum_{\text{ev}} P_a(\theta_C) \sin \phi_C \end{bmatrix}, \quad (32)$$

where the sum is made over all the events inside the same θ_H , ϕ_H bin (all θ_C , all ϕ_C).

The ϕ_H interval was divided into eight bins of 45° each. In each of these bins, Eq. (32) can be written in a matrix form as

$$\underline{e}_i = \underline{F}_i^{-1} \underline{B}_i, \quad (33)$$

where i runs over the ϕ_H bins. The covariance matrices are then given by

$$\underline{V}(\underline{e}_i) = \underline{F}_i^{-1}, \quad \underline{V}(\underline{B}_i) = \underline{F}_i. \quad (34)$$

In this case, the \underline{e} 's are related indirectly to the Wolfenstein parameters through Eqs. (13) and (14). A fit of the ϕ_H distribution of the \underline{e} 's is necessary and was made (a) with five parameters D , R , A , P/P_b , and PP_b if the beam polarization was unknown, and (b) with only four if P_b was known. We had therefore (16 - number of parameters) degrees of freedom. The contribution to the χ^2 per ϕ_i bin is given by

$$\underline{\Delta e}^T [\underline{V}(\underline{e})]^{-1} \underline{\Delta e} = \underline{\Delta e}^T \underline{F} \underline{\Delta e} \quad (35)$$

if

$$\underline{\Delta e} = \underline{e}^m - \underline{e}^c \quad (36)$$

when m and c denote measured or calculated. Here the index i has been dropped for simplicity.

However, as the distribution inside a ϕ_H bin

for all ϕ_H and ϕ_C accepted by the system. This defines the so-called "large" acceptance. Such an event is shown in Fig. 6(b). Figure 6(c) shows also the number of accepted events as a function θ_H . A gain in statistics for scattering angles larger than 6° in the laboratory with respect to the restricted acceptance case is obtained.

In Ref. 16, we showed that the quantities $C(\phi_H)$ and $S(\phi_H)$ defined in Eqs. (13) and (14) can be calculated for fixed ϕ_H bins with the following efficient estimators:

was not uniform, we have taken into account its three first moments. As is shown below, this can be done in a simple way with the estimators we have chosen. Another of their advantages is that they allow corrections for remaining chamber misalignments to be incorporated. These *a posteriori* corrections, different for each ϕ_H bin, were due to skewed planes and irregular wire spacing, effects which were difficult to take into account in the general alignment procedure described in Sec. IVA. These misalignments between the middle and rear telescopes could be measured with events scattered from the LH_2 target but unscattered in the carbon target. For each θ_H , ϕ_H bin, we set

$$\underline{\Delta} = \begin{bmatrix} \Delta_n \\ \Delta_s \end{bmatrix} = \begin{bmatrix} \langle \theta_C \cos \phi_C \rangle \\ \langle \theta_C \sin \phi_C \rangle \end{bmatrix}. \quad (37)$$

The $\underline{\Delta}(\theta_H, \phi_H)$ create parasitic asymmetries of the form

$$\underline{\Delta} \frac{d}{d\theta} (\ln \sigma_C) = \underline{\Delta} \frac{\sigma'_C}{\sigma_C}, \quad (38)$$

where σ_C is the carbon differential cross section.¹⁷ The observed distribution, after the second scattering, becomes [see Eqs. (7), (11)–(14), and (31)]

$$I_C(\phi_H, \theta_C, \phi_C) = I_H(\phi_H) I_{OC}(\theta_C) \left\{ 1 + P_a(\theta_C) \left[C(\phi_H) - \frac{\sigma'_C}{\sigma_C} \Delta_n \right] \cos \phi_C + P_a(\theta_C) \left[S(\phi_H) - \frac{\sigma'_C}{\sigma_C} \Delta_s \right] \sin \phi_C \right\} A(\phi_H, \theta_C, \phi_C). \quad (39)$$

In a ϕ_H bin centered at ϕ_0 , the components of \underline{B} [see Eq. (32)] can be estimated

$$\frac{1}{k} \sum_{\text{ev}} P_a(\theta_C) \cos \phi_C \approx \int_{\Delta\phi_H} C(\phi_H) f_{cc}(\phi_H) d\phi_H + \int_{\Delta\phi_H} S(\phi_H) f_{sc}(\phi_H) d\phi_H - \Delta_n \delta_{cc} - \Delta_s \delta_{sc}, \quad (40)$$

$$\frac{1}{k} \sum_{\mathbf{eV}} P_a(\theta_C) \sin \phi_C \approx \int_{\Delta \phi_H} C(\phi_H) f_{sc}(\phi_H) d\phi_H + \int_{\Delta \phi_H} S(\phi_H) f_{ss}(\phi_H) d\phi_H - \Delta_n \delta_{sc} - \Delta_s \delta_{ss}, \quad (41)$$

where k is the number of incident particles. The misalignments Δ are assumed not to vary inside a bin. The f 's are

$$\begin{aligned} f_{cc}(\phi_H) &= I_H(\phi_H) \int I_{0C}(\theta_C) P_a(\theta_C)^2 d\theta_C \int_0^{2\pi} A(\phi_H, \theta_C, \phi_C) \cos^2 \phi_C d\phi_C, \\ f_{sc}(\phi_H) &= I_H(\phi_H) \int I_{0C}(\theta_C) P_a(\theta_C)^2 d\theta_C \int_0^{2\pi} A(\phi_H, \theta_C, \phi_C) \cos \phi_C \sin \phi_C d\phi_C, \\ f_{ss}(\phi_H) &= I_H(\phi_H) \int I_{0C}(\theta_C) P_a(\theta_C)^2 d\theta_C \int_0^{2\pi} A(\phi_H, \theta_C, \phi_C) \sin^2 \phi_C d\phi_C, \end{aligned} \quad (42)$$

and δ_{cc} is estimated by

$$\begin{aligned} k\delta_{cc} &= k \int_{\Delta \phi_H} I_H(\phi_H) d\phi_H \int I_{0C}(\theta_C) \frac{\sigma'_C}{\sigma_C}(\theta_C) P_a(\theta_C) d\theta_C \int_0^{2\pi} A(\phi_H, \theta_C, \phi_C) \cos^2 \phi_C d\phi_C \\ &\approx G_{cc} = \sum_{\mathbf{eV}} P_a(\theta_C) \frac{\sigma'_C}{\sigma_C}(\theta_C) \cos^2 \phi_C. \end{aligned} \quad (43)$$

Similar equations hold for δ_{sc} and δ_{ss} , and a symmetric matrix \underline{G} can be defined as

$$\underline{G} = k \begin{bmatrix} \delta_{cc} & \delta_{sc} \\ \delta_{sc} & \delta_{ss} \end{bmatrix}. \quad (44)$$

The integrals involved in Eqs. (40) and (41) can be developed further to take into account the ϕ_H dependence inside one ϕ_H bin, centered at ϕ_0 . $C(\phi_H)$ and $S(\phi_H)$ can be approximated with a parabolic shape

$$C(\phi_H) = C_0 + (\phi_H - \phi_0)C_1 + (\phi_H - \phi_0)^2 C_2, \quad S(\phi_H) = S_0 + (\phi_H - \phi_0)S_1 + (\phi_H - \phi_0)^2 S_2. \quad (45)$$

The terms of Eqs. (40) and (41) can be written in the form

$$k \int_{\Delta \phi_H} C(\phi_H) f_{\alpha\beta}(\phi_H) d\phi_H = kC_0 \int f_{\alpha\beta}(\phi_H) d\phi_H + kC_1 \int (\phi_H - \phi_0) f_{\alpha\beta}(\phi_H) d\phi_H + kC_2 \int (\phi_H - \phi_0)^2 f_{\alpha\beta}(\phi_H) d\phi_H \quad (46)$$

$$\approx C_0 F_{0\alpha\beta} + C_1 F_{1\alpha\beta} + C_2 F_{2\alpha\beta}, \quad (47)$$

with

$$F_{icc} = \sum_{\mathbf{eV}} P_a^2(\phi_H - \phi_0)^l \cos^2 \phi_C, \quad F_{iss} = \sum_{\mathbf{eV}} P_a^2(\phi_H - \phi_0)^l \sin^2 \phi_C, \quad F_{isc} = \sum_{\mathbf{eV}} P_a^2(\phi_H - \phi_0)^l \sin \phi_C \cos \phi_C \quad (48)$$

for $l=0, 1, 2$. The F_0, F_1, F_2 matrices are symmetric as is \underline{G} [see Eq. (44)]. Finally Eq. (33) (or its inverse) can be generalized by

$$\begin{aligned} \underline{B}_i &= \begin{bmatrix} \sum_{\mathbf{eV}} P_{ai} \cos \phi_C \\ \sum_{\mathbf{eV}} P_{ai} \sin \phi_C \end{bmatrix} \\ &\approx \underline{F}_{0i} \underline{e}_{0,i} + \underline{F}_{1i} \underline{e}_{1,i} + \underline{F}_{2i} \underline{e}_{2,i} - \underline{G}_i \underline{\Delta}_i. \end{aligned} \quad (49)$$

Then an estimator of $\underline{e}_{0,i}$ becomes

$$\begin{aligned} \underline{e}_{0,i} &= \begin{bmatrix} C(\phi_{0,i}) \\ S(\phi_{0,i}) \end{bmatrix} \\ &= \underline{F}_{0,i}^{-1} (\underline{B}_i + \underline{G}_i \underline{\Delta}_i) - (\underline{F}_{0,i}^{-1} \underline{F}_{1,i}) \underline{e}_{1,i} \\ &\quad - (\underline{F}_{0,i}^{-1} \underline{F}_{2,i}) \underline{e}_{2,i}. \end{aligned} \quad (50)$$

This is the equation that has been used in the evaluation of the results presented here. The corrections \underline{e}_1 and \underline{e}_2 for binning in ϕ_H have been obtained using Eq. (45) and by an iterative fitting procedure. Equation (35) giving the contribution to the χ^2 is written in the same form, the definition of e_0 has to be taken from Eq. (50). If sets of data with different beam polarizations have been recorded, the χ^2 contributions are summed over the different sets. For each θ_H, ϕ_H bin, fourteen sums are necessary: two for \underline{B} , three for \underline{G} , and nine for \underline{F}_i as shown in Table III.

It is not necessary to take into account the angular resolution in the carbon scattering as the carbon analyzing power used already includes these effects. Modifications to the parameters $D, R, A,$ and P due to the θ angular resolution in the first scattering have been calculated.¹¹

TABLE IV. Beam polarization values, as well as χ^2 per degree of freedom. The difference between the polarization parameter P_{n000} , averaged over the whole angular range, and the correspondingly averaged hydrogen analyzing power A_{00n0} is indicated in the last line.

Energy (MeV)	312	392	493	575
type of beam	Scattered	Scattered	Scattered	Accelerated
P_b	0.4147 ± 0.0080	0.4219 ± 0.0063	0.4131 ± 0.0060	0.6560 ± 0.0080
$\chi^2/\text{d.f.}$	0.580	0.663	0.873	0.850
$A_{00n0} - \bar{P}_{n000}$	$+0.0087 \pm 0.0110$	-0.0203 ± 0.0103	-0.0281 ± 0.0100	-0.0201 ± 0.0100

The size of the angular resolution function was determined from unscattered events passing through the hydrogen target. The measured standard deviations were 4.50, 3.99, 3.64, and 3.50 mrad at 312, 392, 493, and 575 MeV, respectively. The corrections, which are insensitive to the shape and to the cuts applied to the resolution function, were most important in the Coulomb-nuclear interference region.

The θ -binning effects have been calculated from the moments of the measured θ_H distribution. The corrections are small, <0.01 for $\theta_{lab} > 4^\circ$ and <0.001 for $\theta_{lab} > 6^\circ$, and are less than the statistical errors. Uncertainties in the corrections have a negligible influence on the final results.

C. Background subtraction

Corrections for the events coming from the Mylar windows of the target appendix and vacuum tank had to be made. Therefore data with an empty target vessel were recorded. The subtractions were done directly on the sums discussed above and not on the asymmetries because the acceptance function for the H_2 events is different from that for events from the Mylar windows. The generalization of Eq. (33) to the dummy subtraction gives

$$\underline{e} = \left(\underline{F}_t - \frac{k_t}{k_b} \underline{F}_b \right)^{-1} \left(\underline{B}_t - \frac{k_t}{k_b} \underline{B}_b \right) \quad (51)$$

and

$$\underline{Y}(\underline{e}) = \left(\underline{F}_t - \frac{k_t}{k_b} \underline{F}_b \right)^{-1} \left[\underline{F}_t + \left(\frac{k_t}{k_b} \right)^2 \underline{F}_b \right] \times \left(\underline{F}_t - \frac{k_t}{k_b} \underline{F}_b \right)^{-1}, \quad (52)$$

with the subscripts t and b referring to the target full and empty, respectively, and k being the number of incident particles. Detailed calculations can be found in Ref. 16.

V. RESULTS

A. Carbon analyzing power

As discussed in Secs. IIB and IVB, knowledge of the quantity $P_b P_C(\theta_C) = P_a(\theta_C)$ is necessary in

order to extract the Wolfenstein parameters P , D , R , and A . Therefore we have measured with the same experimental apparatus single scattering on carbon. Details about the experiment, analysis, and results are discussed in Ref. 17.

B. Beam polarization

As discussed in Sec. IIB, the quantity $\alpha(\theta_H) = P_b A_{00n0}(\theta_H)$ [see Eq. (10)] was measured using events which scattered from the hydrogen target. The quantity $\beta(\theta_H) = P_{n000}(\theta_H)/P_b$ was measured with the distribution after the second scattering [see Eq. (17)]. If parity and time-reversal invariance are imposed, $A_{00n0} = P_{n000} = P$; therefore the beam polarization P_b can be determined from pairs of different measurements of $P(\theta_H)$ for fixed θ_H value, i.e.,

$$P_1(\theta_H) = \alpha(\theta_H)/P_b \quad \text{and} \quad P_2(\theta_H) = \beta(\theta_H)P_b. \quad (53)$$

If σ_α^2 and σ_β^2 are the variances of α and β , respectively, the χ^2 function to be minimized is

$$\chi^2 = \sum_k \frac{[P_1(\theta_H)_k - P_2(\theta_H)_k]^2}{\sigma_1^2 + \sigma_2^2}, \quad (54)$$

where the sum is over the different k bins in θ_H .

The results of the fit are given in Table IV. Figure 7 shows the two measurements of $P(\theta_H)$ after adjustment of P_b at 493 MeV. The small values of $\chi^2/\text{d.f.}$ show that very good compatibility between the results is observed at all energies.

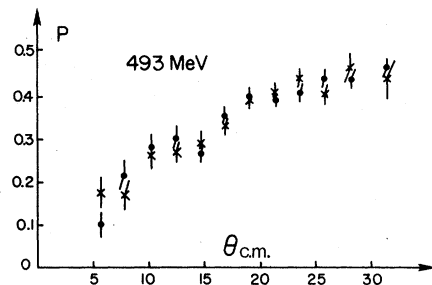


FIG. 7. Compatibility between analyzing power (x) and polarization (●) at 493 MeV.

TABLE V. D , R , A , and P parameters for p - p elastic scattering at 312 MeV, and corresponding values for $d\sigma/d\Omega$ predicted from the Saclay phase-shift analysis (PSA) (Ref. 19).

θ_{lab} (degrees)	$\theta_{\text{c.m.}}$ (degrees)	$d\sigma/d\Omega$ (mb/sr) from PSA (Ref. 19)	P	D	R	A
2.00	4.32	31.80	0.017 ± 0.015	0.916 ± 0.065	0.900 ± 0.065	0.217 ± 0.055
3.00	6.48	7.01	0.122 ± 0.017	0.487 ± 0.096	0.399 ± 0.099	0.056 ± 0.063
4.00	8.64	4.02	0.126 ± 0.019	0.236 ± 0.114	-0.124 ± 0.114	0.025 ± 0.068
5.00	10.80	3.55	0.243 ± 0.017	0.157 ± 0.103	-0.280 ± 0.109	-0.105 ± 0.062
6.00	12.95	3.50	0.250 ± 0.015	0.299 ± 0.090	-0.205 ± 0.092	-0.154 ± 0.055
7.00	15.11	3.52	0.275 ± 0.015	0.424 ± 0.088	-0.218 ± 0.085	-0.232 ± 0.050
8.00	17.26	3.54	0.303 ± 0.013	0.255 ± 0.073	-0.088 ± 0.075	-0.231 ± 0.045
9.00	19.41	3.57	0.354 ± 0.012	0.283 ± 0.066	-0.057 ± 0.067	-0.329 ± 0.041
10.00	21.56	3.60	0.372 ± 0.012	0.356 ± 0.068	-0.193 ± 0.063	-0.255 ± 0.038
11.00	23.71	3.62	0.378 ± 0.012	0.388 ± 0.067	-0.203 ± 0.061	-0.294 ± 0.038
12.00	25.86	3.65	0.377 ± 0.013	0.356 ± 0.074	-0.066 ± 0.061	-0.368 ± 0.039
13.00	28.00	3.66	0.401 ± 0.017	0.328 ± 0.089	0.027 ± 0.067	-0.330 ± 0.042
14.25	30.67	3.69	0.424 ± 0.020	0.226 ± 0.109	0.041 ± 0.074	-0.242 ± 0.046

The three independent values of P_b for the scattered beam were consistent, showing that no significant depolarization effects occur while degrading the beam energy. The best fit for P_b from all three energies simultaneously is

$$P_b = 0.4165 \pm 0.0043. \quad (55)$$

The error includes the statistical error of the fit (0.0040) as well as uncertainty in the product $P_b P_c = P_a$ (0.0015). The beam polarization of the accelerated beam at 575 MeV is also shown in Table IV.

This method provided both a test of our apparatus and of the proportionality of the hydrogen analyzing power and the polarization parameter. An idea of the good compatibility observed at all energies over the whole angular range is given by the very good χ^2 per degree of freedom, as shown in Table IV. Since the precision of our measurements is not sufficient to be a meaning-

ful test of parity and time-reversal violation, the comparison should be considered only as a test of the apparatus. Predictions for $(P_{n000} - A_{00n0})$ by Bryan *et al.*¹⁸ for p - p scattering are small (<0.05) in our angular and energy domain.

C. Parameters D , R , A , and P

Once the beam polarization value was known, values for D , R , A , and P at 312, 392, 493, and 575 MeV (kinetic energy of the reaction) were obtained as explained in Sec. IV B. In the "large" acceptance case [see Sec. IV B 2 (ii) and Eq. (47)] the fits converged without any problem. There is small correlation between P and D parameters, which can be as large as 20%, when P is large. This can be easily explained from the structure of the equations used. These results are given in Tables V–VIII, along with the differential-cross-section values obtained using the Saclay

TABLE VI. Same as Table V but at 392 MeV.

θ_{lab} (degrees)	$\theta_{\text{c.m.}}$ (degrees)	$d\sigma/d\Omega$ (mb/sr) from PSA (Ref. 19)	P	D	R	A
2.00	4.39	22.91	-0.013 ± 0.020	1.024 ± 0.096	0.907 ± 0.096	0.108 ± 0.068
3.00	6.60	6.90	0.098 ± 0.021	0.352 ± 0.130	0.405 ± 0.127	-0.178 ± 0.091
4.00	8.79	4.86	0.208 ± 0.022	0.170 ± 0.134	0.344 ± 0.129	-0.184 ± 0.097
5.00	10.99	4.45	0.211 ± 0.019	0.357 ± 0.112	-0.001 ± 0.115	-0.115 ± 0.082
6.00	13.18	4.32	0.298 ± 0.017	0.358 ± 0.102	-0.037 ± 0.101	-0.181 ± 0.073
7.00	15.38	4.26	0.314 ± 0.016	0.318 ± 0.091	-0.107 ± 0.089	-0.203 ± 0.064
8.00	17.57	4.22	0.348 ± 0.014	0.513 ± 0.083	-0.225 ± 0.081	-0.333 ± 0.057
9.00	19.76	4.20	0.387 ± 0.013	0.488 ± 0.073	-0.058 ± 0.070	-0.308 ± 0.051
10.00	21.94	4.17	0.411 ± 0.013	0.336 ± 0.073	-0.010 ± 0.066	-0.301 ± 0.047
11.00	24.13	4.15	0.442 ± 0.013	0.485 ± 0.072	0.016 ± 0.065	-0.198 ± 0.046
12.00	26.31	4.13	0.450 ± 0.015	0.646 ± 0.077	0.123 ± 0.065	-0.217 ± 0.047
13.00	28.49	4.10	0.453 ± 0.020	0.659 ± 0.100	0.072 ± 0.073	-0.245 ± 0.051
14.25	31.20	4.08	0.437 ± 0.023	0.539 ± 0.111	0.225 ± 0.080	-0.056 ± 0.056

TABLE VII. Same as Table V but at 493 MeV.

θ_{lab} (degrees)	$\theta_{\text{c.m.}}$ (degrees)	$d\sigma/d\Omega$ (mb/sr) from PSA (Ref. 19)	P	D	R	A
2.00	4.49	16.12	0.032 ± 0.030	0.866 ± 0.142	0.843 ± 0.143	0.052 ± 0.112
3.00	6.74	6.78	0.162 ± 0.025	0.386 ± 0.162	0.521 ± 0.163	-0.124 ± 0.132
4.00	8.99	5.65	0.246 ± 0.023	0.677 ± 0.152	0.424 ± 0.153	-0.295 ± 0.121
5.00	11.23	5.36	0.276 ± 0.020	0.574 ± 0.132	0.229 ± 0.126	-0.173 ± 0.099
6.00	13.47	5.21	0.285 ± 0.017	0.870 ± 0.110	0.384 ± 0.110	-0.196 ± 0.088
7.00	15.71	5.09	0.287 ± 0.016	0.680 ± 0.101	0.515 ± 0.098	-0.254 ± 0.077
8.00	17.95	4.98	0.356 ± 0.014	0.570 ± 0.090	0.295 ± 0.088	-0.300 ± 0.068
9.00	20.18	4.89	0.405 ± 0.013	0.591 ± 0.080	0.378 ± 0.080	-0.114 ± 0.062
10.00	22.42	4.81	0.392 ± 0.013	0.756 ± 0.080	0.228 ± 0.075	-0.141 ± 0.058
11.00	24.64	4.73	0.445 ± 0.014	0.732 ± 0.080	0.276 ± 0.073	-0.177 ± 0.056
12.00	26.87	4.66	0.406 ± 0.016	0.667 ± 0.089	0.270 ± 0.074	-0.167 ± 0.057
13.00	29.09	4.59	0.464 ± 0.020	0.666 ± 0.106	0.342 ± 0.081	-0.131 ± 0.063
14.25	31.86	4.51	0.451 ± 0.024	0.631 ± 0.123	0.461 ± 0.090	-0.061 ± 0.070

phase-shift analysis.¹⁹ This latter information is helpful since it is always the product of the differential cross section times a polarization parameter that is expressed as a function of the scattering amplitudes. Results for the "restricted" acceptance are very consistent and can be found in Ref. 12. Figures 8–10 show our results for the parameters D , R , and A as a function of the c.m. scattering angle. As expected, the values of the parameters D and R increase significantly with energy. For example, at $\theta_{\text{c.m.}} \approx 10^\circ$, the value of D increases with 0.35 to 0.80 between 392 and 575 MeV. On the other hand, the A parameter decreases in absolute value as the energy increases. Other available data are also reported in the figures. Notice that very few data points were available at small angles, especially for the A parameter where the only avail-

able data point was at 316 MeV measured by Simmons.²⁰ The two curves shown correspond to the Saclay phase-shift predictions made with different data sets: the dashed line is obtained with the data available in 1976, the full line includes our data and the BASQUE group results²¹ as well as the latest Argonne results on $\Delta\sigma_L$ (Refs. 1–3), $\Delta\sigma_t$,²² and A_{00hh} (Ref. 23) parameter. In the new prediction, the error corridor (not shown on the figures) is significantly reduced. The average contribution to the χ^2 per point in this latter prediction is indicated in Table IX, as well for our data then for the BASQUE data.²¹ Data points which have been rejected on the basis of too large a χ^2 value are also indicated. The phase shifts are able to give a very good description of all data as indicated by the χ^2 /point value around 1. At $\theta=0^\circ$, the three nonzero nuclear

TABLE VIII. Same as Table V but at 575 MeV.

θ_{lab} (degrees)	$\theta_{\text{c.m.}}$ (degrees)	$d\sigma/d\Omega$ (mb/sr) from PSA (Ref. 19)	P	D	R	A
2.00	4.57	14.32	0.109 ± 0.039	0.767 ± 0.123	0.840 ± 0.126	0.107 ± 0.139
3.00	6.86	7.77	0.172 ± 0.020	0.752 ± 0.124	0.618 ± 0.119	0.078 ± 0.137
4.00	9.14	6.97	0.228 ± 0.017	0.653 ± 0.106	0.313 ± 0.106	-0.069 ± 0.117
5.00	11.42	6.73	0.271 ± 0.014	0.719 ± 0.086	0.728 ± 0.085	-0.283 ± 0.098
6.00	13.70	6.58	0.322 ± 0.013	0.964 ± 0.078	0.591 ± 0.076	-0.155 ± 0.085
7.00	15.98	6.43	0.357 ± 0.012	0.837 ± 0.067	0.734 ± 0.067	-0.258 ± 0.076
8.00	18.25	6.27	0.378 ± 0.011	0.816 ± 0.061	0.541 ± 0.060	-0.257 ± 0.069
9.00	20.52	6.11	0.406 ± 0.010	0.801 ± 0.057	0.559 ± 0.055	-0.170 ± 0.062
10.00	22.79	5.95	0.445 ± 0.011	0.780 ± 0.056	0.579 ± 0.053	-0.177 ± 0.059
11.00	25.05	5.76	0.440 ± 0.012	0.834 ± 0.069	0.565 ± 0.052	-0.132 ± 0.058
12.00	27.31	5.59	0.477 ± 0.013	0.756 ± 0.061	0.565 ± 0.053	-0.104 ± 0.061
13.00	29.56	5.40	0.535 ± 0.019	0.675 ± 0.072	0.555 ± 0.059	-0.015 ± 0.081
14.25	32.37	5.18	0.490 ± 0.032	0.591 ± 0.096	0.578 ± 0.067	-0.101 ± 0.182

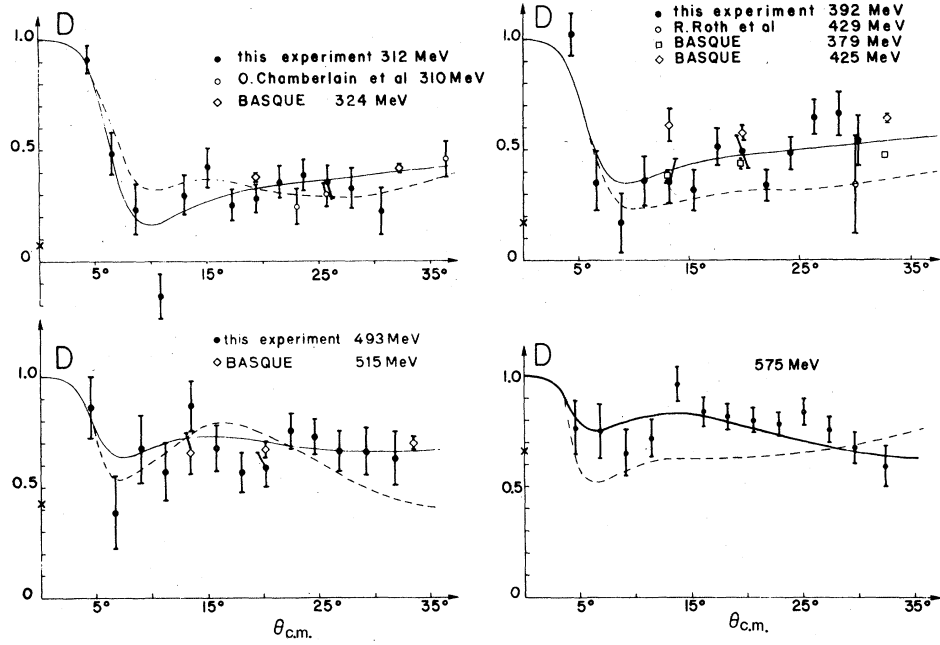


FIG. 8. Wolfenstein parameter D at 312, 392, 493, and 575 MeV compared to other available data. The full line is the present Saclay phase-shift (Ref. 19) prediction. These data are included in the analysis. The 1976 solution is shown as a dashed line. The error corridors (not shown) have reduced significantly. The crosses at zero degree are predictions based on a dispersion analysis by Grein *et al.* (Ref. 24).

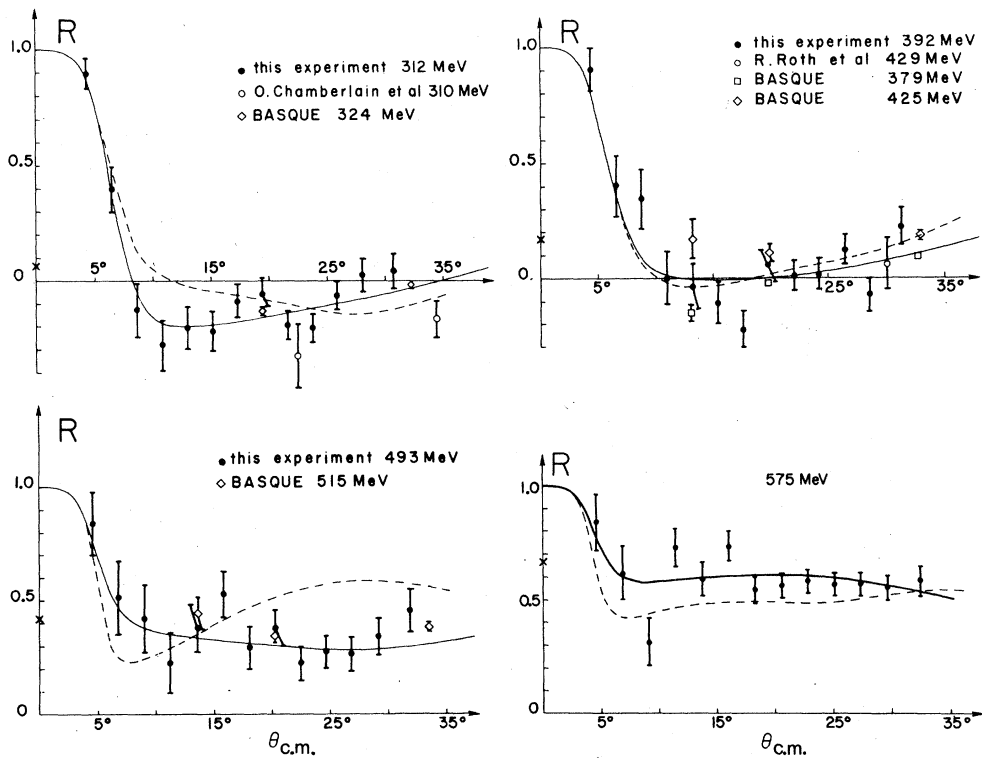


FIG. 9. Wolfenstein parameter R at 312, 392, 493, and 575 MeV. Otherwise, same caption as Fig. 8.

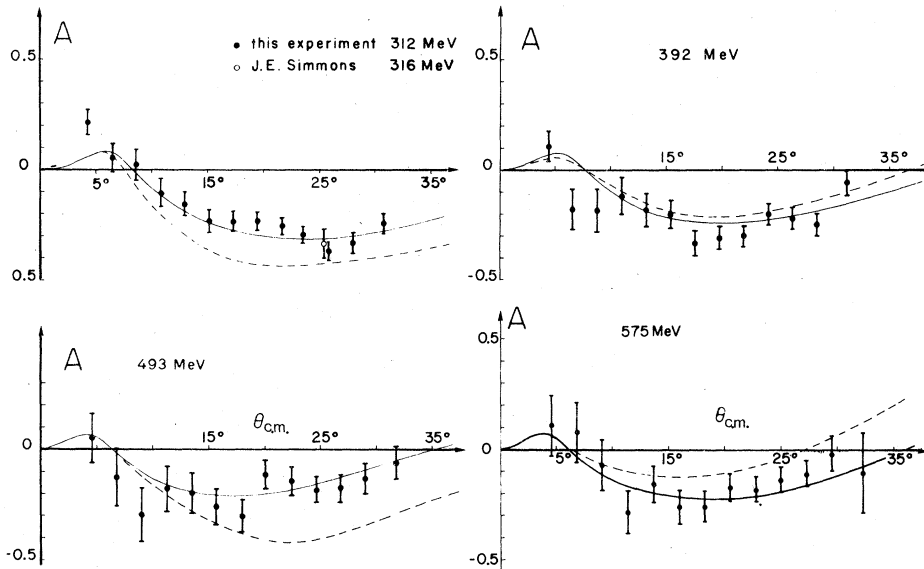


FIG. 10. Wolfenstein parameter A at 312, 392, 493, and 575 MeV. Otherwise same caption as Fig. 8. (At zero degree, A is expected to be zero.)

amplitudes $F_1(0^\circ)$, $F_2(0^\circ)$, and $F_3(0^\circ)$ have been calculated by Grein and Kroll²⁴ using dispersion analysis, which includes the recent Argonne data for total cross sections in spin states $\Delta\sigma_L$ (Refs. 1-3), $\Delta\sigma_t$.²² The nuclear contribution of $D_N(\theta=0^\circ) = R_N(\theta=0^\circ)$ is related to these amplitudes by the relation

$$D_N(\theta=0^\circ) = R_N(\theta=0^\circ) = \frac{4|F_1|^2 - |F_3|^2}{4|F_1|^2 + 2|F_2|^2 + |F_3|^2}. \quad (56)$$

This gives predictions increasing with energy as shown as crosses in Figs. 8 and 9. The extrapolation at $\theta=0^\circ$ of our data seems to agree with

TABLE IX. Average contribution to the χ^2 per point in the Saclay phase-shift analysis (Ref. 19) for our new data on D , R , A , and P as well as for the recent BASQUE results (Ref. 21). Rejected data points, if any, are indicated.

Kinetic energy (MeV)	P	D	R	R'	A
312	1.55	0.72 (without $\theta_{\text{lab}} = 5^\circ$)	0.98	no data	1.25
324 (Ref. 21)	0.82 0.28	0.32	0.60	0.76	no data
379.2 (Ref. 21)	1.03	0.45	2.25 (without $\theta_{\text{lab}} = 13^\circ$)	0.04	no data
392	0.96	1.50	1.69	no data	1.53
424.6 (Ref. 21)	1.84 0.78	0.79	0.36	0.75	no data
493	1.66 (without $\theta_{\text{lab}} = 12^\circ$)	0.88	0.81	no data	0.70
515 (Ref. 21)	1.55 2.26	1.67	0.74	no data	0.78
575	0.90	1.10	1.28	no data	1.31

these predictions.

For the P parameter, the results at 312 MeV are shown in Fig. 11, along with other available ones^{7,25} in the same energy domain. The dotted line is the phase-shift prediction with all available data points included. The full one is a theoretical prediction of the Paris potential.⁴ Our results are in good agreement with phase shift except for the large-angle $P(\theta)$ data for 493 MeV. The last three points are systematically lower than the phase-shift predictions which are constrained very strongly by the BASQUE data²¹ which have small statistical errors. One should note, however, that at 520 MeV, the Alberta point²⁶ at 17°_{lab} with same statistical error as our data is lower than the BASQUE value at 500 MeV.

The parameters P , D , R , and A for scattering from Mylar were also obtained. Because there are several target nuclei with spin zero, the results are interesting. Unfortunately there is a very small background from p - p scattering and there was effectively no energy selection for the scattered proton. The results are given in the Appendix.

D. Systematic errors

Systematic errors were handled as follows:

(i) Most of the systematic errors due to asymmetries in the system can be eliminated by reversing the beam polarization. This was done at 575 MeV, as the incident proton spin was

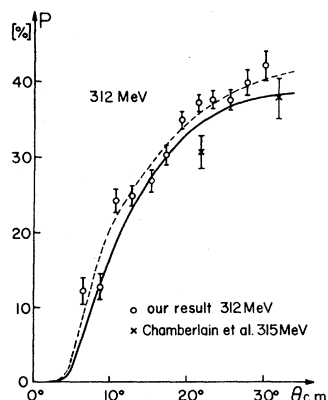


FIG. 11. Polarization parameter P at 312 MeV compared to previous results from Chamberlain (Ref. 25) shown as crosses. The full line is a prediction done with the Paris potential (Ref. 4) at 315 MeV, the dotted line is the Saclay phase-shift (Ref. 19) solution at 312 MeV.

flipped completely. At other energies, 312, 392, and 493 MeV, the spin rotation was less than 180° (see Table I). This small vertical component was taken into account.

(ii) Normalization error due to the estimation of the carbon analyzing power $[P_b P_c(\theta_c)]$ was calculated as a function of θ_H , taking into account the energy dependence and carbon scattering-angle distributions. Little dependence on θ_H was found. A global relative normalization error, of ~ 1 – 1.5% for D , R , and A and 0.5 – 0.8% for P , is present simultaneously at all angles and all parameters for each energy, but this was not included in the error bars.

(iii) The cuts applied on the TOF may introduce parasitic asymmetries if the reconstructed TOF depends on ϕ_H and ϕ_C . Measurements of these deviations give a maximum systematic effect of $\Delta P < 0.002$, and $\Delta D, \Delta R, \Delta A < 0.005$. The last value is an overestimate, as the effects are corrected when the beam polarization is reversed.

(iv) We have tested the sensitivity to the TOF cuts by evaluating the D , R , A , and P parameters for two different cuts. Virtually identical results were obtained.

(v) Contamination due to three-body inelastic reactions was considered. Cuts on TOF and dE/dx measurements eliminated inelastic events for which a proton or a deuteron was detected. However, pions have velocities similar to the elastically scattered protons and it was impossible to distinguish them. A Monte Carlo study has shown that this contamination in the accepted events was less than 0.3% at 575 MeV. The percentage is smaller at the lower beam energies.

(vi) Effects due to uncertainties in the background subtraction normalization were negligible ($\Delta P < 0.001$, $\Delta D, \Delta R, \Delta A < 0.006$).

This study of systematic errors has shown that they are smaller than the statistical ones.

VI. CONCLUSION

Our measurements of P , D , R , and A at 312, 392, 493, and 575 MeV add 208 new data points in an angular region between 3° and 33° in the c.m. where very little data existed (except for P parameters). Good agreement for the P parameter with other available results was observed. These new data confirm the large energy dependence predicted by phase-shift analysis. A large angular dependence, especially at small angle for D and R , has also been seen for which a good angular resolution was needed. This information was of great help in the phase-shift analyses, which have significantly improved their predictions reducing significantly the error corridor.

TABLE X. D , R , A , and P parameters for proton-Mylar scattering at 312, 392, 493, and 575 MeV. Errors are purely statistical.

Energy (MeV)	θ_{lab} (degrees)	D	R	A	P
312	3.0	0.94 ± 0.11	1.01 ± 0.12	0.15 ± 0.06	0.10 ± 0.02
	5.0	1.04 ± 0.14	0.82 ± 0.14	0.08 ± 0.06	0.37 ± 0.02
	7.0	0.96 ± 0.13	0.68 ± 0.14	0.17 ± 0.06	0.50 ± 0.02
	9.0	0.98 ± 0.17	0.32 ± 0.17	0.23 ± 0.07	0.56 ± 0.03
	11.5	0.72 ± 0.20	0.28 ± 0.17	0.11 ± 0.08	0.61 ± 0.03
392	3.0	0.86 ± 0.13	0.97 ± 0.12	0.21 ± 0.08	0.14 ± 0.02
	5.0	0.96 ± 0.13	0.85 ± 0.12	0.33 ± 0.09	0.33 ± 0.02
	7.0	0.91 ± 0.13	0.80 ± 0.13	0.21 ± 0.10	0.42 ± 0.03
	9.0	0.70 ± 0.17	0.68 ± 0.17	0.16 ± 0.11	0.48 ± 0.03
	11.0	1.01 ± 0.20	0.66 ± 0.20	0.11 ± 0.13	0.50 ± 0.04
493	13.5	0.53 ± 0.33	0.34 ± 0.26	0.23 ± 0.16	0.36 ± 0.07
	3.0	0.98 ± 0.13	1.01 ± 0.13	0.25 ± 0.11	0.18 ± 0.02
	5.0	1.08 ± 0.14	0.87 ± 0.13	0.42 ± 0.11	0.27 ± 0.02
	7.0	0.98 ± 0.15	0.78 ± 0.15	0.10 ± 0.13	0.43 ± 0.03
	9.0	1.15 ± 0.20	1.13 ± 0.20	-0.16 ± 0.15	0.38 ± 0.04
575	11.0	0.61 ± 0.27	0.64 ± 0.23	0.16 ± 0.19	0.36 ± 0.05
	13.5	0.81 ± 0.39	0.88 ± 0.30	0.38 ± 0.26	0.33 ± 0.08
	3.0	1.17 ± 0.10	0.90 ± 0.10	0.06 ± 0.12	0.15 ± 0.02
	5.0	1.03 ± 0.10	0.83 ± 0.10	0.03 ± 0.12	0.26 ± 0.02
	7.0	0.87 ± 0.12	0.62 ± 0.12	0.27 ± 0.15	0.35 ± 0.02
	9.0	0.94 ± 0.15	0.92 ± 0.16	0.03 ± 0.16	0.37 ± 0.03
	11.0	0.86 ± 0.23	0.54 ± 0.20	0.18 ± 0.24	0.38 ± 0.05
	13.5	1.02 ± 0.30	0.39 ± 0.24	0.14 ± 0.30	0.34 ± 0.09

ACKNOWLEDGMENTS

We would like to thank Professor E. Heer for his constant encouragement. We thank the Swiss Institute for Nuclear Research for its generous technical assistance, and especially its director, Professor J. P. Blaser. We thank CERN and the University of Neuchâtel for lending us their sole-noids. The assistance of the computing staff at the Federal Institute of Technology at Lausanne, as well as that of the computing staff at the Geneva Cantonal Hospital, was greatly appreciated. This work could not have been done without the aid of the technical staff of the University of Geneva, especially that of S. Morenzoni. We thank also Dr. P. Zoldos for his help during the early stage of experiment, and Professor A. Gersten for many useful discussions and exchange of information. This work was supported by the Swiss National Funds and the "Convention Intercantonale d'Enseignement du 3ème Cycle de la Physique en Suisse Romande."

APPENDIX: PARAMETERS D , R , A , AND P ON MYLAR

As explained in Sec. IV C data with an empty target vessel were recorded. They consisted of p -Mylar ($C_5H_4O_2$) scattering. One can apply the same analysis procedure to those data only, in

order to extract the D , R , A , and P parameters. Results are given in Table X, but in 2° bins in angle laboratory as the available statistics was low. It would be interesting to subtract the p - p contribution in order to be left only with information on scattering from the spin-zero nuclei ^{12}C and ^{16}O where the relations

$$P^2 + R^2 + A^2 = 1, \quad (A1)$$

$$D = 1 \quad (A2)$$

should hold. As the p - ^{12}C and p - ^{16}O differential

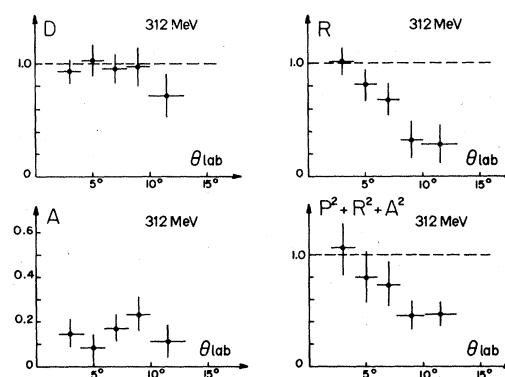


FIG. 12. Wolfenstein parameters D , R , and A for proton-Mylar scattering at 312 MeV.

cross sections are as much as 2 orders of magnitude larger than for p - p scattering, and elastic scattering is dominant at small angles, the results should approximately obey relations (A1) and (A2). The data for 312 MeV are presented in Fig. 12, where deviations from Eqs. (A1) and (A2) occur for

$\theta_{lab} \gtrsim 5^\circ$. This can be due to the fact that inelastically scattered events have not been rejected. One notices that at all energies, the A parameter on Mylar is always positive, which is to be compared to the always negative values obtained for p - p scattering.

- *Present address: Stanford University, Calif. 94305.
 †Present address: Nuclear Research Center, University of Alberta, Edmonton, Canada T6G 2N5.
 ‡Present address: Landis & Gyr AG, Zug, Switzerland.
- ¹I. P. Auer, E. Colton, H. Halpern, D. Hill, H. Spinka, G. Theodosiou, D. Underwood, Y. Watanabe, and A. Yokosawa, *Phys. Rev. Lett.* **41**, 354 (1978).
²I. P. Auer, E. Colton, D. Hill, K. Nield, B. Sandler, H. Spinka, Y. Watanabe, and A. Yokosawa, *Phys. Lett.* **67B**, 113 (1977).
³I. P. Auer, A. Beretvas, E. Colton, D. Hill, K. Nield, H. Spinka, D. Underwood, Y. Watanabe, and A. Yokosawa, *Phys. Lett.* **70B**, 475 (1977).
⁴R. Vinh-Mau, in *Nucleon-Nucleon Interactions—1977*, Proceedings of the Second International Conference, Vancouver, edited by H. Fearing, D. Measday, and A. Strathdee (AIP, New York, 1978).
⁵C. de Tar, *Phys. Rev. D* **17**, 323 (1978).
⁶D. Aebischer, B. Favier, L. G. Greeniaus, R. Hess, A. Junod, C. Lechanoine, J. C. Niklès, D. Rapin, C. Richard-Serre, and D. W. Werren, *Phys. Rev. D* **13**, 2478 (1976).
⁷D. Aebischer, B. Favier, L. G. Greeniaus, R. Hess, A. Junod, C. Lechanoine, J. C. Niklès, D. Rapin, and D. W. Werren, *Nucl. Phys.* **A276**, 445 (1977).
⁸J. Bystricky and F. Lehar, in *Physik Daten Karlsruhe* Report No. 11-1, 1978, edited by G. Ebel and H. Behrens (unpublished).
⁹J. Bystricky, F. Lehar, and P. Winternitz, *J. Phys. (Paris)* **39**, 1 (1978).
¹⁰D. Aebischer, R. Bovet, B. Favier, L. G. Greeniaus, R. Hess, A. Junod, C. Lechanoine, B. Mauron, J. C. Niklès, D. Rapin, J. P. Vittet, and D. W. Werren, *Nucl. Instrum. Methods* **117**, 131 (1974).
¹¹D. Rapin, Ph. D. thesis No. 1884, University of Geneva, Switzerland, 1978 (unpublished).
¹²B. Favier, Ph.D. thesis No. 1894, University of Geneva Switzerland, 1978 (unpublished).
¹³D. Besset, Q. H. Do, B. Favier, L. G. Greeniaus, E. Heer, R. Hess, C. Lechanoine, D. Rapin, and D. W. Werren (unpublished).
¹⁴J. C. Niklès, Ph.D. thesis No. 1747, University of Geneva, Switzerland, 1976 (unpublished).
¹⁵D. Besset, Q. H. Do, B. Favier, L. G. Greeniaus, R. Hess, C. Lechanoine, D. Rapin, D. W. Werren and Ch. Weddigen, in *Nucleon-Nucleon Interactions—1977*, (Ref. 4), p. 50.
¹⁶D. Besset, B. Favier, L. G. Greeniaus, R. Hess, C. Lechanoine, D. Rapin, and D. W. Werren, *Nucl. Instrum. Methods* **166**, 515 (1979).
¹⁷D. Besset, Q. H. Do, B. Favier, L. G. Greeniaus, R. Hess, C. Lechanoine, D. Rapin, D. W. Werren, and Ch. Weddigen, *Nucl. Instrum. Methods* **166**, 379 (1979).
¹⁸R. Bryan and A. Gersten, *Phys. Rev. Lett.* **26**, 1000 (1971).
¹⁹J. Bystricky, C. Lechanoine, and F. Lehar, Saclay Report No. 1-79 (unpublished).
²⁰J. E. Simmons, *Phys. Rev.* **104**, 416 (1956).
²¹D. V. Bugg, J. A. Edgington, C. Amsler, R. C. Brown, C. J. Oram, K. Skakarchi, N. M. Stewart, G. A. Ludgate, A. S. Clough, D. Axen, S. Jaccard, and J. Vavra, *J. Phys. G* **4**, 1025 (1978).
²²E. K. Biegert, J. A. Buchanan, J. M. Clement, W. H. Dragoset, R. D. Felder, J. H. Hoftiezer, K. R. Hogstrom, J. Hudomalj-Gabitzsch, J. D. Lesikar, W. P. Madigan, G. S. Mutchler, G. C. Phillips, J. B. Roberts, and T. M. Williams, *Phys. Lett.* **73B**, 235 (1978).
²³I. P. Auer, A. Beretvas, E. Colton, H. Halpern, D. Hill, K. Nield, B. Sandler, H. Spinka, G. Theodosiou, D. Underwood, Y. Watanabe, and A. Yokosawa, *Phys. Rev. Lett.* **41**, 1436 (1978).
²⁴W. Grein and P. Kroll, *Nucl. Phys.* **B137**, 173 (1978).
²⁵O. Chamberlain, E. Segré, R. D. Tripp, C. Wiegand, and T. Ypsilantis, *Phys. Rev.* **105**, 288 (1957).
²⁶L. G. Greeniaus, D. A. Hutcheon, C. A. Miller, G. A. Moss, G. Roy, R. Dubois, C. Amsler, B. K. S. Koene, and B. T. Murdoch, *Nucl. Phys.* **A322**, 308 (1979).